THE JOURNAL OF BIOLOGICAL CHEMISTRY VOL. 281, NO. 37, pp. 26813–26820, September 15, 2006

Escherichia coli CorA Periplasmic Domain Functions as a Homotetramer to Bind Substrate*[S]

Received for publication, March 13, 2006, and in revised form, July 10, 2006 Published, JBC Papers in Press, July 11, 2006, DOI 10.1074/jbc.M602342200

Shi-Zhen Wang[1], **Yong Chen**[1], **Zhan-Hua Sun, Qiang Zhou, and Sen-Fang Sui**[2]

From the Department of Biological Sciences and Biotechnology, State-Key Lab of Biomembranes and Membrane Biotechnology, Tsinghua University, Beijing 100084, China

CorA is a primary Mg^{2+} transporter in bacteria, which also mediates influx of Ni^{2+} and Co^{2+}. Topological studies suggested that it could be divided into a large soluble periplasmic domain (PPD) and three membrane-spanning α-helixes. In the present study, glutathione *S*-transferase (GST) fusion *Escherichia coli* CorA PPD was purified by GST affinity chromatography, and PPD was obtained by on-column thrombin digestion. Size-exclusion chromatography indicated that purified PPD exists as a homotetramer. Single particle electron microscopy analysis of PPD and two-dimensional crystals of GST-PPD indicated that *E. coli* CorA PPD is a pyramid-like homotetramer with a central cavity. Comparison of the CD spectra of full-length CorA and PPD also suggested that PPD has similar secondary structure to the full-length CorA. Dissociation constants for CorA and PPD with their substrates, determined by dose-dependent fluorescence quench of ligands, suggested that purified PPD retains its substrate binding ability as native CorA. The CorA PPD structure described here may provide structural information for the *E. coli* CorA functional oligomeric state.

Magnesium is the most abundant intracellular divalent cation (1, 2) and is required for many important cellular functions, including acting as an essential cofactor for numerous enzymatic reactions (3, 4), maintaining genomic stability (2), modulating signal transduction (5, 6), and playing a role in energy metabolism (7) and cell proliferation (8).

So far, three magnesium transport systems have been identified in bacteria: CorA, MgtA/B, and MgtE (9–15). *CorA* is the first identified gene mediating Mg^{2+} influx (16, 17) and by far the most abundant prokaryotic magnesium transporter (18–20). It shares no sequence homology with any other known membrane protein or transporter families (10, 21). Its homologs are also widespread in archaea, fungi, yeast, plants, and mammals (22). The best studied CorA systems are from *Salmonella Typhimurium* and *Escherichia coli*. *S. Typhimurium CorA* encodes a membrane protein of 316 amino acid residues, with a unique topology (21). It can be considered as a two-domain protein: a 235-amino acid residue N-terminal-soluble domain, which is located in the periplasmic space (periplasmic domain (PPD)[3]), followed by a transmembrane domain (TM) composed of three transmembrane segments (21). However, recent work by Daley and colleagues (23) revealed that both the N and C termini of *E. coli* CorA are located at the cytosol side. From the small number of TM segments, it is reasonable to suggest that CorA would function as an oligomer. Recent studies suggested that CorA from *Salmonella* serovar *Typhimurium*, *Methanococcus jannaschii*, and *Bacillus subtilis*, expressed in the cells and purified in the PPD, all exist as homotetramers (24).

Primary structural and functional studies indicate that CorA is unusual among secondary transporters. It expresses constitutively and transports Mg^{2+} with high capacity. The transporting kinetics of *S. typhimurium* CorA has been studied in detail (17, 25). It not only uptakes Mg^{2+}, Co^{2+}, and Ni^{2+} but also mediates Mg^{2+} efflux when extracellular magnesium concentration is higher than 1 mM (25). Site-directed mutagenesis revealed that three conserved residues on the α-helices of TM2 and TM3 participate directly in the transporting process and may be involved in substrate binding and formation of a specific Mg^{2+}-permeable pore (26, 27). Cobalt(III) hexa-amine, an analog of hydrated Mg^{2+}, can inhibit CorA specifically, which implies that it is hydrated Mg^{2+} that binds to the N-terminal periplasmic domain in the first step of transporting Mg^{2+} (28).

Although CorA is the most widely studied magnesium transporter in bacteria, little is known about its structural and molecular roles of the large N-terminal PPD in Mg^{2+} transport. In the present study, we focused on the structure and function of PPD. Soluble PPD was purified and biochemically characterized. Size-exclusion chromatography showed that purified PPD exists as a tetramer. A combination of CD spectra and substrate-binding assay showed that CorA PPD retained the same substrate binding capacity as the full-length native protein. The structure observed by electron microscopy revealed the overall architecture of PPD tetramers in solution and on the lipid membrane. The pyramid-like homotetramer of CorA PPD with a central cavity may connect with the "magnesium pore," thus forming a "tunnel" that mediates ion transport.

* This work was supported by the National Nature Science Foundation of China (Grants 30340420442 and 30330160) and the National Basic Research Program of China (Grant 2004CB720005). The costs of publication of this article were defrayed in part by the payment of page charges. This article must therefore be hereby marked "*advertisement*" in accordance with 18 U.S.C. Section 1734 solely to indicate this fact.

[S] The on-line version of this article (available at http://www.jbc.org) contains additional text, references, Table S1, and Figs. S1 and S2.

[1] Both authors contributed equally to this work.

[2] To whom correspondence should be addressed. Tel.: 86-10-6278-4768; Fax: 86-10-6279-3367; E-mail: suisf@mail.tsinghua.edu.cn.

[3] The abbreviations used are: PPD, periplasmic domain; DDM, *n*-dodecyl-β-D-maltoside; GST, glutathione *S*-transferase; TM, transmembrane domain; TBS, Tris-buffered saline; IQ, index quality.

TABLE 1
Plasmids and primers used in the current work

Name	Vector	Primers used in cloning or site mutagenesis	Reference
CorAH	pBAD-mycHisA	5-CATGCCATGGGAAGCGCATTTCAACTGGAAAA-3 5-GGGCCCAAGCTTGGATCCACGCGGAACCAGCCAGTTCTTCCGCTTAAA-3	29
PPD	pGEX-4T-1	5-GGAGGGATCCACCATGGGAAGCGCATTTCAAC-3 5-GCAGGAATTCTCAGATATCTCGCAGGATTTC-3	This work
C191A	pGEX-4T-1	5-GGAGGGATCCACCATGGGAAGCGCATTTCAAC-3 5-GCAGGAATTCTCAGATATCTCGCAGGATTTC-3 5-GTATCCATCAGAGCCAGGCGAACTT-3 5-AAGTTCGCCTGGCTCTGATGGATAC-3	This work

MATERIALS AND METHODS

Protein Expression and Purification—All *E. coli* cells were grown in Luria-Bertani broth, containing 100 μg/ml ampicillin. Plasmids and primers used in the present work are listed below (Table 1). PPD and C191A were expressed with an N-terminal GST fusion tag in *E. coli* strain BL21(DE3), which was induced by 0.1 mM isopropyl 1-thio-β-D-galactopyranoside at 20 °C for 6 h when A_{600} reached 0.6. Harvested cells were suspended in phosphate-buffered saline buffer (140 mM NaCl, 2.7 mM KCl, 10 mM Na_2HPO_4, 1.8 mM KH_2PO_4), containing 5 mM β-mercaptoethanol, 2 mM phenylmethylsulfonyl fluoride, 1.5 kilo-unit DNaseI, 1 mg/ml Lysozyme, then broken by ultrasonic homogenizer. The supernatant was obtained by centrifuged cell lysates at 34,000 × *g* for 45 min at 4 °C. PPD and C191A were obtained by GST affinity purification and on column thrombin digestion at 16 °C for 8 h, and then concentrated by ultrafiltration. GST-PPD was obtained by eluting the bound protein directly from glutathione-Sepharose (Amersham Biosciences) after extensive washing. Affinity-purified PPD and C191A were further loaded onto a Superdex 200 column (Amersham Biosciences), eluted with TBS (50 mM Tris-HCl, pH 8.0, 100 mM NaCl) containing 5 mM β-mercaptoethanol, and collected as 0.4 ml per tube by an auto collector. The peak eluted at ~132 kDa was collected and concentrated by ultrafiltration for subsequent electron microscopy analysis, CD scan, and substrate binding assay.

The full-length CorA was purified using a previously reported protocol with minor modifications: 5 mM β-mercaptoethanol was added to all buffers used in the purification process (29), and size-exclusion chromatography was performed on a Superdex 200 column (Amersham Biosciences) using TBS containing 20%(v/v) glycerol, 0.1% DDM, 5 mM β-mercaptoethanol as running buffer.

Electron Microscopy and Image Processing—Two-dimensional crystals of GST-PPD on monolayers were obtained using the techniques described by Uzgiris *et al.* (30) and in our previous work (31, 32). 100 μg/ml affinity purified GST-PPD in the buffer (50 mM Tris-HCl, pH 8.0, 100 mM NaCl, 5 mM β-mercaptoethanol) was incubated underneath the monolayer composed of *E. coli* total lipid extract for 24 h at 15 °C. After incubation, the lipid monolayers were picked up on hydrophobic carbon-coated electron microscopy grids and negatively stained with 1% uranyl acetate for 1 min. To observe CorA PPD molecules in solution, 3 μl of PPD protein sample with a concentration of 20 μg/ml was directly dropped onto a carbon-coated, glow-charged electron microscopy grid for ~1 min, and then negatively stained with 1% uranyl acetate for 1 min.

The specimens were examined with a Phillips CM120 microscope operated at 100 kV. The low dose mode was used to take images using Kodak SO-163 films at 74,000× magnification. Films were developed in full-strength D19 for 12 min. Images were digitized on a Nikon Coolscan 9000ED scanner at a step size of 12.7 μm/pixel.

The processing of GST-PPD two-dimensional crystals was performed using the ICE (33)and MRC Image Processing Package (34) as described, including Fourier transformation, indexing, lattice parameter refinement, lattice unbending, amplitude, and phase extraction. The symmetry of the crystal was calculated by the ALLSPACE program (35).

For reconstruction of CorA-PPD in solution, the EMAN package was used (36) and images were processed following standard protocols. 9768 particles were selected and extracted by the BOXER program. The optical density histograms for the pixels in each image were scaled to the mean ± S.D. for all images. Particle images were low-pass-filtered to 1 nm and then centered and rotationally aligned against an average of all non-aligned images. A new reference was calculated using the aligned images, and iterations of alignment and averaging were repeated another four times. The aligned particles were classified into ~80 groups using factor analysis with k-means grouping. The initial model was created by common lines approach and refined by projection matching with 4-fold symmetry imposed. After several cycles of refinement, the process was halted because the Fourier shell correlation with the previous model did not yield any substantial differences within the resolution cutoff. The final map was calculated from 8143 particles. The resolution was estimated by applying the 0.5 threshold to the Fourier shell correlation between two maps calculated from two halves of the data.

Circular Dichroism—CD spectra were obtained on a Jasco J-715 spectropolarimeter. PPD and C191A were diluted to 0.2 mg/ml with buffer containing 20 mM Hepes-NaOH, pH 7.0, 100 mM NaCl and analyzed in a 1-mm path length and 200 μl of cells at 25 °C. The same procedure was applied to full-length CorA, which was diluted to 0.2 mg/ml with the same buffer containing additional 20%(v/v) glycerol and 0.1% DDM. Samples were scanned five times at a rate of 200 nm/min and averaged. All spectra were subtracted by their buffer spectra. Calculations of the fractional percentage of secondary structures were carried out using the computer programs Spectra-Manager (Jasco), CD-Deconvolution and Dicroprot.

Substrate Binding Measured by Fluorescence Quenching—The dissociation constants of CorA and PPD to different substrates were measured by the ligand dose-dependent fluores-

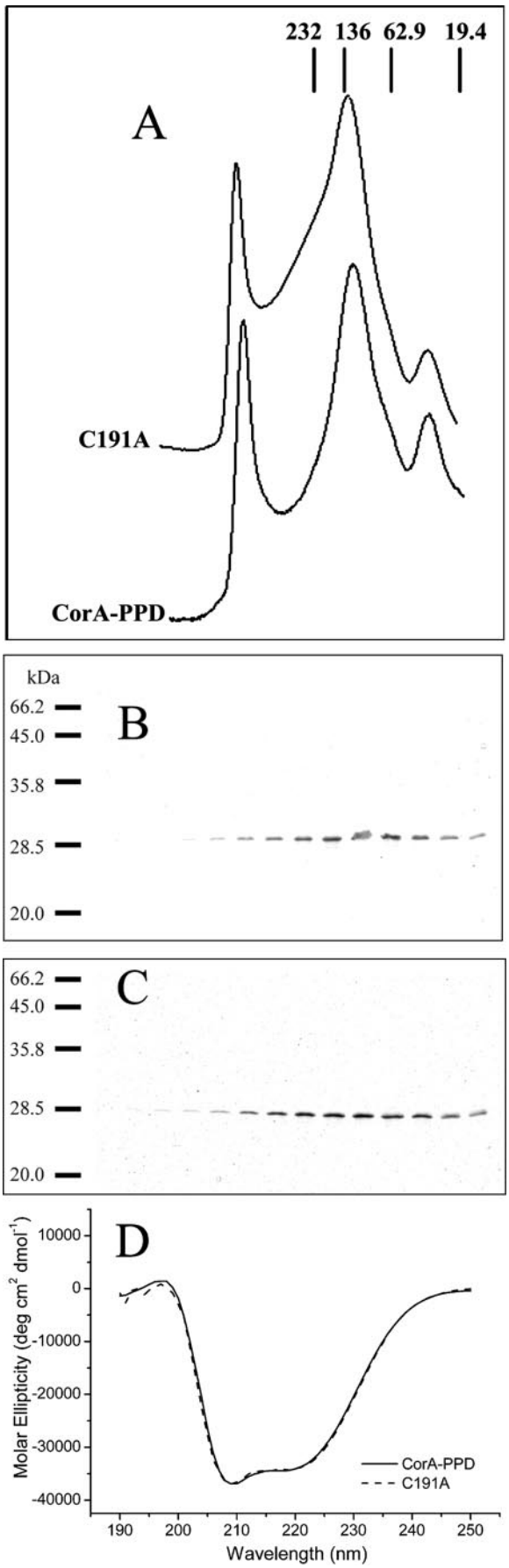

cence quenching method. An excitation wavelength of 283 nm and an emission range of 295–425 nm were set on a Hitachi F-4500 fluorescence meter. The measurements were performed using protein samples diluted to 0.1 mg/ml with 20 mM Hepes-NaOH, 100 mM NaCl, pH 7.0 (adding 20% glycerol and 0.1% DDM in dilution buffer for CorA) and titrated by stock ligands in a 0.7-ml quartz cuvette at 25 °C. Volume changes of titration were omitted because they were controlled within 2.5%, and the final concentrations of Mg^{2+}, Ni^{2+}, Co^{2+}, Ca^{2+}, and Zn^{2+} were 1 mM. Fluorescence intensities at the emission apexes were exported. The fluorescence quenching ΔF *versus* ligands concentration [*S*] was plotted. K_d(app) of CorA and PPD to Mg^{2+}, Ni^{2+}, and Co^{2+} were calculated by performing curve-fitting with the SigmaPlot9.0 program using a simple binding mode according to Equation 1,

$$\Delta F = (F_0 - F) = [\Delta F_{max}][S]/(K_{d(app)} + [S]) \qquad \text{(Eq. 1)}$$

where F is the fluorescence intensity at emission peaks following titration of substrates to concentration [*S*], F_0 is the fluorescence intensity of protein samples at the emission peak in the absence of ligands, and K_d(app) is the apparent dissociation constant of CorA or CorA-PPD to ligands.

RESULTS

CorA-PPD Exists as Homotetramer—Based on topology studies of *S. Typhimurium* CorA, which has only an 8-amino acid residue difference compared with *E. coli* CorA, the CorA PPD was expressed by the encoding region from Met-1 to Ile-223 in *E. coli*. Previously, PPD from *Salmonella* serovar *Typhimurium* and *Methanococcus jannaschii* were purified and refolded from inclusion bodies produced in *E. coli* (24). We also found *E. coli* CorA PPD normally formed inclusion bodies when expressed alone or with a 6× histidine tag. In the present work, soluble PPDs were obtained by expressed with an N-terminal GST fusion tag and purified by performing GST affinity chromatography and on column digestion. Size-exclusion chromatography analysis of affinity-purified PPD detected three peaks: aggregated form (≫232 kDa, full exclusion), presumed homotetramer (≈132 kDa), and monomer (between 66 and 19.4 kDa), respectively (Fig. 1*A*). No dimer peak was

FIGURE 1. **Size-exclusion analysis of GST affinity-purified PPD and C191A.** *A*, elution curve of GST affinity chromatography-purified CorA PPD and C191A. Analysis was performed on an AKTA purifier (Amersham Biosciences). Protein samples were loaded into a 100-μl sample loop and injected into a Superdex 200 preparation column that was equilibrated and eluted with TBS buffer containing 5 mM β-mercaptoethanol. Data analysis and curve editing were performed using Unicore 5.01 software. A total of three peaks were detected in effective separation volume, estimated by standard, corresponding to the aggregated form, homotetramer and monomer of CorA-PPD, respectively. Three standard proteins were catalase (232 kDa), dimer (132 kDa), and monomer (66 kDa) of albumin bovine V, chymotrypsinogen A (19.4 kDa). *B* and *C*, SDS-PAGE of PPD and C191A samples of gel filtration. 10 μl of protein samples was mixed with 5× loading buffer, loaded onto the 12.5% SDS-PAGE. The gels were stained with Coomassie Brilliant Blue R-250, then scanned into and edited with Photoshop 7.0. *D*, CD of CorA PPD and C191A. CD spectra were obtained on a Jasco J-715 spectropolarimeter. Presumed PPD and C191A tetramer collection were diluted to 0.2 mg/ml with 20 mM Hepes-NaOH, pH 7.0, containing 100 mM NaCl and analyzed in a 1-mm path length 200-μl cell at 25 °C. All spectra were subtracted from their buffer spectra, and then converted to molar ellipticity. No obvious difference in secondary structure was observed between PPD and C191A.

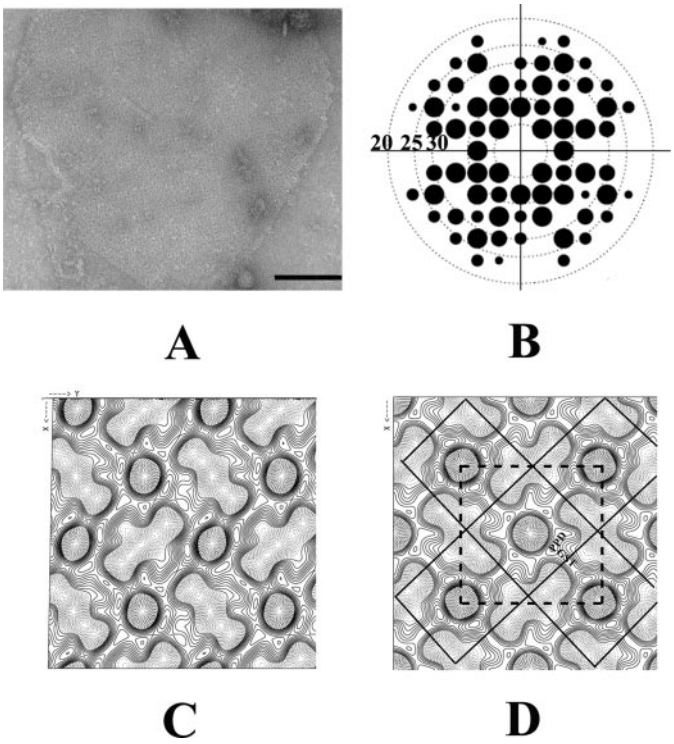

FIGURE 2. **Crystallographic analysis of GST-fused CorA PPD 2D crystals.** *A*, the two-dimensional crystals of GST-fused CorA PPD formed on *E. coli* phospholipid monolayers. The crystals were formed by incubating 100 μg/ml GST-PPD in TBS containing 5 mM β-mercaptoethanol underneath an *E. coli* total lipid extract monolayer for 24 h at 15 °C. The *bar* is 100 nm. *B*, computed Fourier transform of a GST-PPD two-dimensional crystal after two-round unbending. The resolution circles representing 20, 25, and 30 Å are indicated. Only *spots* with an IQ of <4 are displayed, and the *size of the spot* is inversely proportional to IQ: IQ 1 is the largest, and IQ 4 is the smallest. The resolution can reach 20 Å. *C*, the projection map of a GST-PPD two-dimensional crystal without symmetry enforcement. *D*, the projection map of CorA two-dimensional crystal with *p*4 symmetry imposed at a cut-off resolution of 20 Å. The lattice parameters are a = b = 120 Å, γ = 90°. The central unit cell is indicated by a *dashed square*, and five tetrameric structures are marked by *solid squares*. The possible PPD and GST positions are indicated.

detected. A site-directed mutant, C191A, with its Cys-191 (the only cysteine in *E. coli* PPD) to alanine mutation, was also purified. Size-exclusion chromatography showed that it could also form a homotetramer with the same chromatographic pattern as PPD (Fig. 1, *A*–*C*). Further comparison of the CD spectra from PPD and C191A indicated that no large differences in secondary structure existed (Fig. 1*D*).These results indicate that disulfide bonds do not participate in tetramer formation. Although some PPD dimers were detected by native PAGE and unreduced SDS-PAGE (data not shown), these dimers were perhaps misfolded rather than in a stable oligomeric state.

The oligomeric structure of PPD was further confirmed by two-dimensional crystals formed on lipid monolayers. We tried several different PPD constructs and found they could form some ordered structure on lipid monolayers composed of native *E. coli* lipid whole extract. When GST-PPD was incubated with *E. coli* lipid monolayer for 24 h, a kind of square crystal formed (Fig. 2*A*). Electron micrographs of the best negatively stained two-dimensional crystal diffracted to 20 Å (Fig. 2*B*). The lattice parameters were determined to be a = b = 122 Å, γ = 90°. Symmetry analysis suggested strong *p*4 or *p*4212 symmetry (Table 2). The projection maps without any symmetry and with *p*4 symmetry imposed are shown in Fig. 2 (*C* and *D*). There were no significant differences between these two maps, indicating that CorA two-dimensional crystals have real *p*4 symmetry. The projection map in Fig. 2*D* shows one unit cell (the *dashed square*) containing eight high density domains around the 4-fold axis. Four inner high density domains are arranged to form a square structure with a central low density cavity. The dimension of the square is ~7 × 7 nm. There are a total of five tetrameric rings shown in Fig. 2*D*, and each of them is marked by a *solid square*. The possible existence of a gliding axis (*p*4212) indicates that the four rings distributed around the central ring are in an upside-down orientation, and different staining effects from the two sides makes the internal tetramer

TABLE 2
Phase residuals (°) of a typical image calculated for 17 layer groups by Allspace

Layer group		Phase residue (no.) *versus* other spots (90° random)		Phase residue (no.) *versus* theoretical (45° random)		Target residual based on statistics taking the Friedel weight into account
1	p1	19.7	82	14.2	82	
2	p2	30.4[a]	41	15.2	82	28.5
3b	P12_b	70.8	29	37.2	2	20.0
3a	P12_a	79.0	31	28.7	6	20.6
4b	P121_b	12.1[b]	29	2.4	2	20.0
4a	P121_a	10.4[b]	31	32.2	6	20.6
5b	C12_b	70.8	29	37.2	2	20.0
5a	C12_a	79.0	31	28.7	6	20.6
6	P222	61.1	101	16.0	82	23.3
7b	P2221b	53.9	101	37.3	82	23.3
7a	P2221a	59.6	101	38.8	82	23.3
8	P22121	19.2[b]	101	15.4	82	23.3
9	C222	61.1	101	16.0	82	23.3
10	p4	16.3[b]	105	15.3	82	23.1
11	P422	52.2	219	15.6	82	21.4
12	P4212	13.0[b]	219	15.3	82	21.4
13	p3	40.9	40			19.7
14	P312	35.2	106	12.2	16	20.4
15	P321	34.9	105	10.4	14	20.3
16	p6	38.2	121	15.2	82	22.7
17	P622	34.6	252	15.2	82	21.2

[a] Should be considered.
[b] Acceptable.

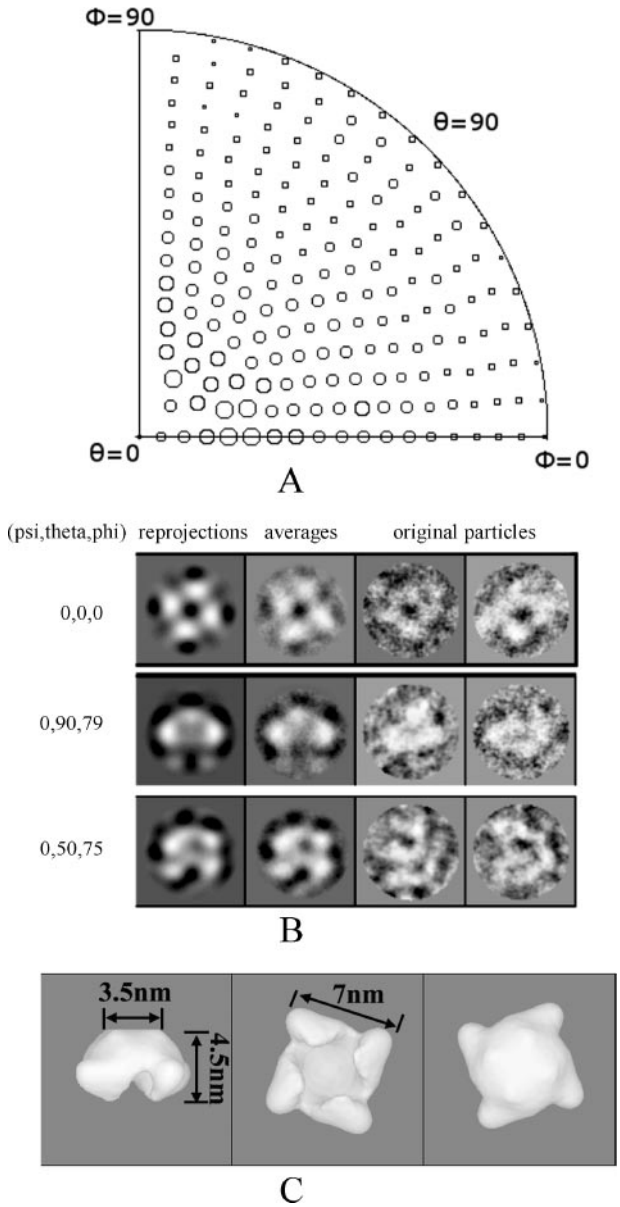

FIGURE 3. **The structure of CorA PPD in solution.** *A*, the Euler angle distribution of the final reconstruction, showing there is no preferred orientation for CorA PPD particles on carbon film. Each *circle* represents a class, and the *diameter* of *each circle* is positively related to the particle numbers in this class. *B*, some distinct views from the final model. The *panel* shows, from *left* to *right*, reprojections from the model, the corresponding averages, and examples of raw particles assigned to this class. The *box length* is 12.3 nm. *C*, the reconstructed three-dimensional map of *E. coli* CorA PPD. The surface representations were rendered and displayed by WEB. Three views are shown and from *left* to *right*, the *medium* and *right views* were obtained after the 90° rotation operation of the *left view* around the *horizontal axis*. The *box length* is 12.3 nm.

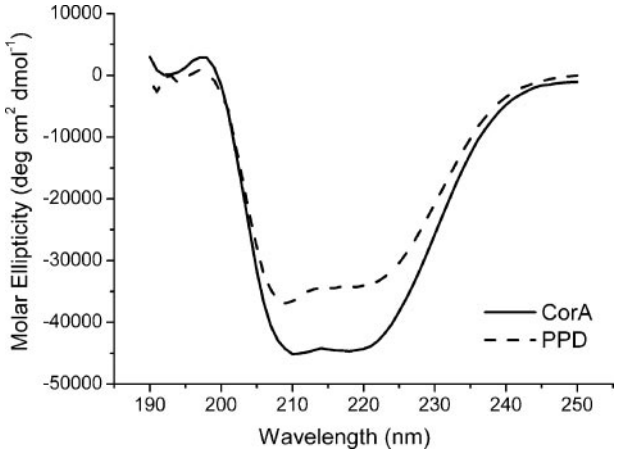

FIGURE 4. **CD of CorA PPD and full-length CorA.** CD spectra were obtained on a Jasco J-715 spectropolarimeter. CorA PPD and CorA were diluted to 0.2 mg/ml with 20 mM Hepes-NaOH, pH 7.0, containing 100 mM NaCl and analyzed in a 1-mm path length 200-μl cell at 25 °C, the same procedure for CorA except additional 20% (v/v) glycerol and 0.1% (w/v) DDM in dilution buffer. All spectra were subtracted from their buffer spectra, and then converted to molar ellipticity. Both CD spectra of CorA and PPD were featured by two peaks at 209 and 220 nm, the typical peaks of α-helix.

different from the surrounding four. The GST might account for the bridge density connecting two adjacent subunits.

Electron microscopy single particle analysis could provide the overall architecture of CorA PPD in solution. The negatively stained PPD in solution showed intact particles without any preferred orientation, as shown by the angular distribution map (Fig. 3*A*). Some particles showed the square shape as that showed in two-dimensional density maps (Fig. 3*B*, *first row*). We obtained the three-dimensional structure of PPD from negative-stained protein particles in solution by single particle reconstruction. The common line method was used to get an initial model, and the projection match was performed to refine the model. The initial model showed a little distortion of the 4-fold symmetry. Because the GST-CorA two-dimensional crystal showed strong 4-fold symmetry, the *C*4 symmetry was enforced in the refinement steps. A stable three-dimensional model was obtained after eight iterations of alignment/classification/three-dimensional reconstruction cycles and included 8143 particles. Some class averages and corresponding reprojections, together with some raw particles, are shown in Fig. 3*B*. The high similarity between the averages and reprojections indicates the accuracy of the three-dimensional reconstruction. The resolution test performed on two independent data sets give a value of 2.8 nm for the Fourier shell correlation criterion (0.5). The overall architecture of the PPD shows a pyramid shape with a central cavity (Fig. 3*C*). The length of the top side is 3.5 nm, and the length of the bottom side is 7 nm. The height is 4.5 nm. Four bulges derived from four CorA-PPD subunits are arranged symmetrically around the central cavity. The projection of this structure along the 4-fold symmetry axis has similar dimensions (~7 nm) and arrangement of high density domains as the projection map from the GST-PPD two-dimensional crystals, indicating they have the same oligomeric structure. All of these results reveal that the tetramer is the basic oligomeric state of PPD *in vitro*.

CorA-PPD Has Similar Secondary Structure with Full-length CorA—To further evaluate the influence of TM truncation on the structure of PPD, CD spectra of full-length CorA and PPD were scanned and compared. Results showed that CD spectra of CorA and PPD were both characterized by two negative peaks at ~209 and 220 nm, the typical features of α-helix (Fig. 4). Secondary structure prediction using CD spectra-based computer programs showed that, although a little different, both CorA and PPD consist of ~30 ~ 40% α-helix and 20% β-sheet. Differences between CD spectra of CorA and PPD may be partly due to the truncation of C-terminal membrane-spanning

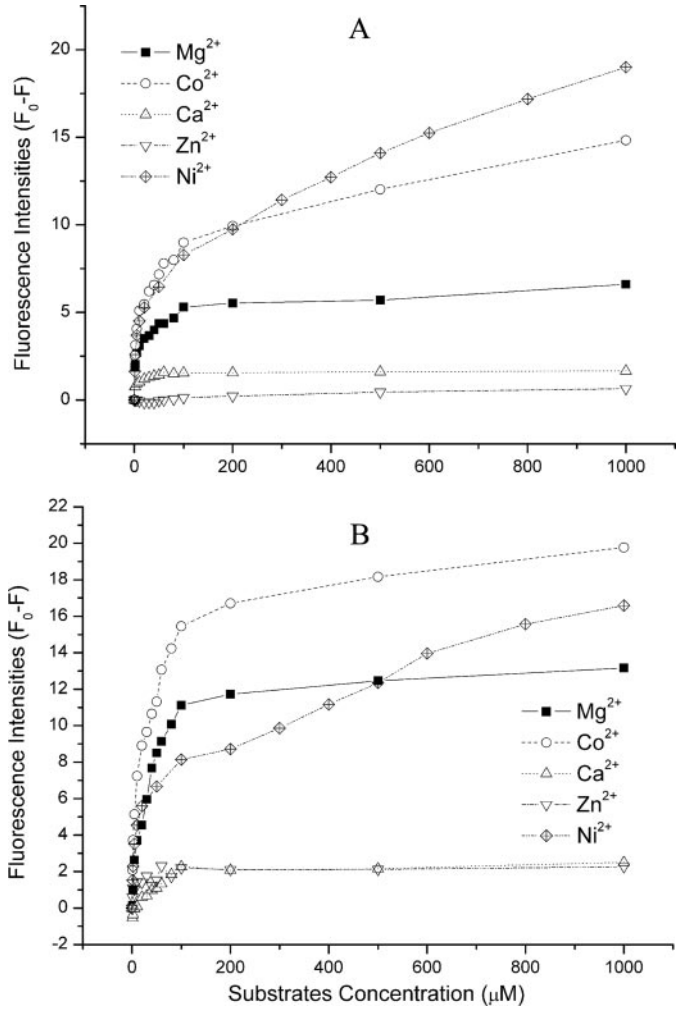

FIGURE 5. **Ligand dose-dependent fluorescence quenching of CorA and CorA PPD.** Ligand dose-dependent fluorescence quench assays of CorA and CorA PPD were performed on an F-4500 fluorescence meter (Hitachi, Japan). The excitation wavelength was set at 283 nm, and data of emission from 295 to 425 nm were collected. The assays were performed using protein samples diluted to 0.1 mg/ml with 20 mM Hepes-NaOH, 100 mM NaCl, pH 7.0 (adding 20% glycerol and 0.1% DDM in dilution buffer for CorA) in a 0.7-ml cuvette at 25 °C. Intrinsic fluorescence intensities gradually decreased following titration. Fluorescence intensities at emission apexes of CorA (*A*) and PPD (*B*) *versus* substrates concentration were plotted.

α-helix. PPD, in regard to its secondary structure, seemed to retain its native structure as in full-length CorA.

Purified CorA-PPD Has Substrate Binding Activity—To ensure that the observed pyramid-like structure of PPD was its functional state, the binding capacities of CorA and PPD to their substrates Mg^{2+}, Ni^{2+}, and Co^{2+} were analyzed and compared by the ligand dose-dependent fluorescence quench method. Despite the fact that tryptophan contributes most to protein fluorescence, there are only 4 tryptophans but 22 phenylalanine and 8 tyrosine residues in the sequence, so protein intrinsic fluorescence excited at 283 nm was integrative contributions of tryptophan, phenylalanine, and tyrosine. Generally, titration of substrates would lead to quenching of the PPD intrinsic fluorescence, and the quenching effect showed a ligand dose-dependent mode. The titration measurements were ended when the final ion concentrations reached 1 mM. CorA or PPD were saturated by over 100 μM Mg^{2+}; thereafter, intrinsic fluorescence showed little decrease (Fig. 5, *A* and *B*). Co^{2+} and Ni^{2+} had optical absorbance, which would introduce a progressive inner-filter effect on PPD intrinsic fluorescence, and even a denaturing effect on the protein itself at higher concentrations. Thus the titration curves showed a typical hyperbolic shape at low ion concentration but a linear decrease when ion concentration was >200 μM. Moreover, K_d values were measured more precisely under "tight binding" conditions, which occurred when [*S*] is equal to or slightly higher than K_d and there is an equilibrium between bound and free proteins (37). Therefore, dissociation constants of CorA and PPD for Mg^{2+} and Co^{2+} were calculated in ligands concentration range at 1 ~ 200, for Ni^{2+} at 1 ~ 500 μM. Within this range, optical absorbance and the denaturing effect were relatively negligible as partly indicated by comparison of CD spectra (data not shown). All data were fitted with a one-site saturation mode due to lack of knowledge about the exact substrate binding site of PPD. The apparent dissociation constants (K_d(app)) of CorA for Mg^{2+},Co^{2+}, and Ni^{2+} were 18, 30, and 201 μM, and the K_d of CorA-PPD for Mg^{2+}, Co^{2+}, and Ni^{2+} were 31, 24, and 106 μM, respectively (Table 3). These data are similar to the results of Snavely (25) determined *in vivo*: the K_d of CorA to Mg^{2+}, Co^{2+}, and Ni^{2+}, are within the ranges of 20 ~ 40, 20 ~ 40, and 200 ~ 400 μM, respectively. Besides, we also tested the fluorescence changes of CorA and PPD following titration of Ca^{2+} and Zn^{2+}, and it showed little response, indicating that binding of Mg^{2+}, Ni^{2+}, and Co^{2+} to CorA or PPD were specific (Fig. 5, *A* and *B*). No remarkable differences in dissociation constants to their substrates were observed between CorA and PPD, indicating that pyramid structure of PPD we observed was a functional state.

TABLE 3

The apparent dissociation constant (K_d(app)) of CorA and CorA PPD to Mg^{2+}, Ni^{2+}, and Co^{2+}

K_d(app) were determined by the ligand dose-dependent protein intrinsic fluorescence quench method as described under "Materials and Methods." Curve fitting were performed on EnzymeKinetics1.01 package of SigmaPlot9.0 software by using the one-site saturation mode. 200 iterations were set to all curve fittings, and *R* scores of all curve fittings were over 0.98.

	Mg^{2+}	Ni^{2+}	Co^{2+}
		μM	
CorA	18.4 ± 4.6	201 ± 64.9	29.8 ± 8.8
CorA-PPD	30.9 ± 2.6	106.8 ± 39.9	23.6 ± 3.8

DISCUSSION

Over 90% of the *E. coli* CorA PPD expressed alone or with a His_6 fusion tag in *E. coli* strain BL21(DE3) formed inclusion bodies, and purification of *Salmonella* serovar *Typhimurium* and *M. jannaschii* CorA PPD also had to follow an inclusion body-refolding strategy for the same reason (24). However, when fused with an N-terminal GST tag, up to 70% of the GST-PPD fusion protein was soluble. After affinity purification and removal of the GST fusion tag by thrombin digestion, PPD was soluble and stable. It has been demonstrated that, when the GST tag is fused at the proper terminal with proper linker, it can facilitate the folding process *in vivo*, thereby enhancing the solubility and stability of the target protein (38).

There is only one cysteine (Cys-191) in the whole CorA sequence. Warren (24) suggested that detection of the dimer

band on unreduced SDS-PAGE does not definitely prove the existence of disulfide bonds in the native CorA, for Cys-191 could form a disulfide bond with an introduced Cys-317 residue. A dimer band was also detected in affinity-purified PPD in the present work by native PAGE and unreduced SDS-PAGE (data not shown). Gel-filtration and CD spectra revealed that C191A, a Cys-191 to alanine mutant of PPD, could form homotetramer as well, indicating that Cys-191 is not essential for formation of PPD homotetramer. On the contrary, formation of disulfide bonds might be a sign that the protein is misfolded, which accelerates the aggregation process of PPD. This was demonstrated partly by the facts that the C191A mutant was stabilized in TBS without β-mercaptoethanol, whereas PPD aggregated rapidly when β-mercaptoethanol was absent from the buffer (data not shown). Hence, PPD homotetramer perhaps consists of four independent monomers.

Although purified CorA PPD has a stable structure, whether PPD could retain its native functional structure after truncation of the C-terminal membrane-spanning α-helix remains unknown. In this case, we used CD spectra to compare the structures of CorA-PPD and full-length CorA. CD spectrometry is a convenient way to evaluate the secondary structure of a protein. Secondary structure contents calculated by various computer programs showed that both CorA and PPD are comprised of ~30 ~ 40% α-helix and 20% β-sheet. The α-helix content in PPD was a little lower than CorA due to truncation of the transmembrane α-helix. Furthermore, we scanned CorA and PPD over a buffer pH range from 5.0 to 9.0, and no obvious differences were detected except at pH 5.0, where both CorA and PPD seemed to lose their secondary structure completely (data not shown). The similarity of the CD spectra change again suggested that PPD could perhaps retain its secondary structure when expressed without TM.

Besides structural comparison of CorA-PPD and full-length CorA, we also compared the substrate binding of both proteins. The dissociation constant is a sound parameter for direct estimation of their binding capacity for substrates. The K_d(app) of CorA determined by the ligand dose-dependent fluorescence quench method in the present study were similar to the K_d values measured *in vivo* by Snavely (25). The K_d(app) of PPD to its substrate exhibited no difference compared with CorA, indicating that the purified PPD homotetramer could retain its primary function of substrates binding as CorA.

The pyramid-like structure of PPD revealed by single particle analysis also suggested that PPD was a homotetramer, consistent with our results from size-exclusion chromatography and Warren's previous report on cross-linking (24). Functional analysis of CorA and PPD showed that the observed pyramid-like structure of PPD is its functional and native state, and homotetramer is its functional state.

Although the current structure has low resolution, it can still provide some indication of PPD functions. Previous site-directed mutagenesis analyses (26, 27) of CorA TM2 and TM3 had screened out several conserved amino acid residues influencing the transporting activity of CorA, which may participate in the formation of a "magnesium pore." The observed central stain-filled cavity, together with the magnesium pore composed of transmembrane α-helices, perhaps form a "tunnel" through which ions can flow. The pyramid-like PPD has a wide opening toward the periplasmic space and a narrow neck toward the membrane. The wide opening may facilitate binding of the relatively large hydrated magnesium ion, because it was suggested that magnesium in the hydrated form binds to CorA in the first step of magnesium transport (28). After binding hydrated magnesium, dehydration must occur before the bare magnesium ion can go through the narrow neck of PPD and enter into the magnesium pore formed by transmembrane segments. Some residues in the narrow neck of PPD may participate in the dehydration process and function as molecular filters for selection of the ions. A high resolution structure of CorA PPD is needed to understand how PPD binds, dehydrates, and selects divalent ions.

Sequence alignment showed that *Thermotoga maritima* CorA and *E. coli* CorA share ~18% of identity and >28% similarity. When this report was nearly completed, we noticed that *T. maritima* CorA had been crystallized by two independent groups with different crystallization conditions. One, which had been deposited in the PDB data base (PDB code 2BBJ) at 3.85-Å resolution, showed a pentamer structure of *T. maritima* CorA (39), and another at 4.7-Å resolution revealed 4–6 molecules per asymmetric unit (40). Besides, the 3.85-Å crystal structure also demonstrated that *T. maritima CorA* has only two transmembrane segments. Topological studies by Daley *et al.* (23) suggested that *E. coli* CorA has only two transmembrane segments with its large soluble domain at the cytosol side, which means that the *E. coli* CorA has an identical topology to that of *T. maritima* CorA, rather than that suggested by Smith *et al.* (21). Therefore, we re-evaluated the topological structure of *E. coli* CorA by labeling and detecting 6× histidine fusion tags added to the N and C termini of *E. coli* CorA in intact and 0.2% (w/v) Triton X-100-permeated spheroplasts. The functional assays revealed that CorA with N- or C-terminal 6× histidine tags retained partial transporting activity. We obtained the same results (see data in supplemental materials) as those reported by Smith *et al.* (21), supporting that the N-terminal large soluble domain of *E. coli* CorA was at periplasmic space. Hence, *E. coli* and *T. maritima* CorA may represent different CorA subfamilies of different topology and oligomeric state. Our results indicate that *E. coli* CorA PPD perhaps functions as a homotetramer.

Acknowledgments—We thank Prof. D. N. Wang, from Skirball Institute of the New York University School of Medicine, for supplying us the plasmid of E. coli CorA and for his aid in expressing and purifying E. coli CorA, as well as his critical discussions and suggestions on the present work. We thank Prof. R. C. Gardner, from the University of Auckland, New Zealand, for providing us the S. cerevisiae strain CM66; Dr. H. W. Wang for suggestions on processing the electron microscopy images and reviewing the manuscript; and W. L. Jiang for maintenance of the electron microscope.

REFERENCES

1. Grubbs, R. D., and Maguire, M. E. (1987) *Magnesium* **6,** 113–127
2. Hartwig, A. (2001) *Mutat. Res.* **475,** 113–121
3. Romani, A., Marfella, C., and Scarpa, A. (1993) *Miner. Electrolyte Metab.* **19,** 282–289

4. Romani, A. M., and Scarpa, A. (2000) *Front. Biosci.* **5,** D720–D734
5. White, R. E., and Hartzell, H. C. (1989) *Biochem. Pharmacol.* **38,** 859–867
6. Garcia Vescovi, E., Soncini, F. C., and Groisman, E. A. (1996) *Cell* **84,** 165–174
7. Saris, N. E., Mervaala, E., Karppanen, H., Khawaja, J. A., and Lewenstam, A. (2000) *Clin. Chim. Acta* **294,** 1–26
8. Walker, G. M. (1986) *Magnesium* **5,** 9–23
9. Moncrief, M. B., and Maguire, M. E. (1998) *Infect. Immun.* **66,** 3802–3809
10. Kehres, D. G., Lawyer, C. H., and Maguire, M. E. (1998) *Microb. Comp. Genomics* **3,** 151–169
11. Maguire, M. E. (1992) *J. Bioenerg. Biomembr.* **24,** 319–328
12. Smith, R. L., and Maguire, M. E. (1998) *Mol. Microbiol.* **28,** 217–226
13. Townsend, D. E., Esenwine, A. J., George, J., 3rd, Bross, D., Maguire, M. E., and Smith, R. L. (1995) *J. Bacteriol.* **177,** 5350–5354
14. Tao, T., Snavely, M. D., Farr, S. G., and Maguire, M. E. (1995) *J. Bacteriol.* **177,** 2654–2662
15. Smith, R. L., Thompson, L. J., and Maguire, M. E. (1995) *J. Bacteriol.* **177,** 1233–1238
16. Nelson, D. L., and Kennedy, E. P. (1971) *J. Biol. Chem.* **246,** 3042–3049
17. Hmiel, S. P., Snavely, M. D., Miller, C. G., and Maguire, M. E. (1986) *J. Bacteriol.* **168,** 1444–1450
18. Smith, D. L., and Maguire, M. E. (1993) *Miner. Electrolyte Metab.* **19,** 266–276
19. Roof, S. K., and Maguire, M. E. (1994) *J. Am. Coll. Nutr.* **13,** 424–428
20. Smith, R. L., and Maguire, M. E. (1995) *J. Bacteriol.* **177,** 1638–1640
21. Smith, R. L., Banks, J. L., Snavely, M. D., and Maguire, M. E. (1993) *J. Biol. Chem.* **268,** 14071–14080
22. Gardner, R. C. (2003) *Curr. Opin. Plant Biol.* **6,** 263–267
23. Daley, D. O., Rapp, M., Granseth, E., Melen, K., Drew, D., and von Heijne, G. (2005) *Science* **308,** 1321–1323
24. Warren, M. A., Kucharski, L. M., Veenstra, A., Shi, L., Grulich, P. F., and Maguire, M. E. (2004) *J. Bacteriol.* **186,** 4605–4612
25. Snavely, M. D., Florer, J. B., Miller, C. G., and Maguire, M. E. (1989) *J Bacteriol.* **171,** 4761–4766
26. Szegedy, M. A., and Maguire, M. E. (1999) *J. Biol. Chem.* **274,** 36973–36979
27. Smith, R. L., Szegedy, M. A., Kucharski, L. M., Walker, C., Wiet, R. M., Redpath, A., Kaczmarek, M. T., and Maguire, M. E. (1998) *J. Biol. Chem.* **273,** 28663–28669
28. Kucharski, L. M., Lubbe, W. J., and Maguire, M. E. (2000) *J. Biol. Chem.* **275,** 16767–16773
29. Chen, Y., Song, J., Sui, S. F., and Wang, D. N. (2003) *Prot. Expr. Purif.* **32,** 221–231
30. Uzgiris, E. E., and Kornberg, R. D. (1983) *Nature* **301,** 125–129
31. Wang, H. W., and Sui, S. (2001) *J. Struct. Biol.* **134,** 46–55
32. Wang, H. W., and Sui, S. (1999) *J. Struct. Biol.* **127,** 283–286
33. Hanein, D., Matlack, K. E., Jungnickel, B., Plath, K., Kalies, K. U., Miller, K. R., Rapoport, T. A., and Akey, C. W. (1996) *Cell* **87,** 721–732
34. Crowther, R. A., Henderson, R., and Smith, J. M. (1996) *J. Struct. Biol.* **116,** 9–16
35. Valpuesta, J. M., Carrascosa, J. L., and Henderson, R. (1994) *J. Mol. Biol.* **240,** 281–287
36. Ludtke, S. J., Baldwin, P. R., and Chiu, W. (1999) *J. Struct. Biol.* **128,** 82–97
37. Walmsley, A. (2000) in *Membrane Transport: A Practical Approach* (Baldwin, S. A., ed) pp. 167–192, Oxford University Press Inc., London
38. Smyth, D. R., Mrozkiewicz, M. K., McGrath, W. J., Listwan, P., and Kobe, B. (2003) *Protein Sci.* **12,** 1313–1322
39. Lunin, V. V., Dobrovetsky, E., Khutoreskaya, G., Zhang, R., Joachimiak, A., Doyle, D. A., Bochkarev, A., Maguire, M. E., Edwards, A. M., and Koth, C. M. (2006) *Nature* **440,** 833–837
40. Payandeh, J., and Pai, E. F. (2006) *Acta Crystallogr. Sect. F Struct. Biol. Cryst. Commun.* **F62,** 148–152